Supporting Information

Flexible Silk Film Based on Synergy of Hydrogen Bond and Cross-linking Network for Magnetic Sensitive Skin

Cuiling Zhang,[a#] *Qi Zhang,*[b#] *Xinran Li,*[a] *Wang Zhan,*[a] *Yongliang Han,*[c] *Zeying Zhang,*[a] *Wei Su,*[c] *Li Xue,*[a] *Wei Zhang,*[d] *Ke Zhou,*[d] *Shaoming Pan,*[d] *Niancai Peng,*[e] *Zhilu Ye,*[a*] *Bin Peng,*[c*] *Xiaohui Zhang*[a*]

[a] State Key Laboratory for Manufacturing Systems Engineering, The Key Laboratory of Biomedical Information Engineering of Ministry of Education, Center for Mitochondrial Biology and Medicine, School of Life Science and Technology, International Joint Laboratory for Micro/Nano Manufacturing and Measurement Technology, Xi'an Key Laboratory for Biomedical Testing and High-end Equipment, Xi'an Jiaotong University, Xi'an 710049, Shannxi, P.R. China.

[b] National Local Joint Engineering Research Center for Precision Surgery & Regenerative Medicine, Shaanxi Provincial Key Laboratory of Magnetic Medicine, Department of Hepatobiliary Surgery, The First Affiliated Hospital of Xi'an Jiaotong University, State Key Laboratory for Manufacturing Systems Engineering, Electronic Materials Research Laboratory, Key Laboratory of the Ministry of Education, School of Electronic Science and Engineering, Xi'an Jiaotong University, Xi'an 710049, China.

[c] State Key Laboratory for Manufacturing Systems Engineering, Electronic Materials Research Laboratory, Key Laboratory of the Ministry of Education, Engineering Research Center of Spin Quantum Sensor Chips, Universities of Shaanxi Province, School of Electronic Science and Engineering, Xi'an Jiaotong University, Xi'an 710049, China.

[d] Guangxi Power Grid Equipment Monitoring and Diagnosis Technology Innovation Center, Guangxi Key Laboratory of Intelligent Control and Maintenance of Power Equipment, Electric Power Research Institute of Guangxi Power Grid CO., LTD., Nanning, Guangxi, 530023.

[e] State Key Laboratory for Manufacturing Systems Engineering, School of Instrument Science and Technology, International Joint Laboratory for Micro/Nano Manufacturing and Measurement Technology, Xi'an Key Laboratory for Biomedical Testing and High-end Equipment, Xi'an Jiaotong University, Xi'an 710054, China.

[*] Corresponding author.

[#] Equal contribution.

E-mail address: xiaohuizhang@mail.xjtu.edu.cn, pengbin@xjtu.edu.cn, zhiluye@xjtu.edu.cn

The supporting information contains 21 pages, 14 figures, 1 table, and 1 movie.

Material Characterization.

Fourier transform infrared (FTIR) spectra of the pure silk film and cross-linked silk film was obtained using FTIR spectroscopy (Bruker VERTEX70, USA) with the spectral wavenumber range of 4000~400cm^{-1}. To investigate the crystal structure changes of the films, X-ray diffraction (XRD) was carried out by an X-ray diffractometer (Bruker D8 ADVANC, Germany) with 2θ from 5° to 45°. Thermogravimetric analysis (TGA) of the cross-linked silk film was conducted by Mettler Toledo TGA/DSC3+ (China) operating from 40℃ to 800℃ in nitrogen atmosphere with a heating speed of 10 ℃/min. The surface morphology and roughness of the cross-linked silk film was evaluated using an atomic force microscope (AFM, SPM-9700HT, Japan).

Characterization of Mechanical Properties.

Mechanical properties of the pure silk film and cross-linked silk films were measured using a universal testing machine (CMT1502, China). All the films to be tested were cut into rectangular shape (length of 3 mm, width of 1 mm and thickness of 25 μm).

Water Stability.

To evaluate the water stability of the pure silk film and cross-linked silk film, the films were immersed into 5 mL of deionized water at room temperature. We took photographs of films at 0.5 hours, 6 hours, and 24 hours during the dissolution process. The water stability of the samples was assessed by the residual mass of the film. The residual mass was determined by the Eq. (1):

$$Residual\ mass\ (\%) = \frac{m_t}{m_0} \times 100\% \tag{1}$$

where m_t and m_0 represents the weight of the films at the immersion time is 0 and 24 hours, respectively.

Live-Dead Staining.

The biocompatibility of the silk-based AMR was analyzed by live-dead staining. Briefly, the mouse cardiomyocytes and fibroblasts (1:20) were seeded on the cross-linked silk films and silk-based AMR and cultured for 48 hours. After washing with phosphate buffer solution (PBS), the cells were stained with calcein AM and EthD-1 solution (Biolabo, China) and incubated for 30 min at 37°C. The cell viability and death were visualized under a fluorescence microscope (NIB620-FL, China).

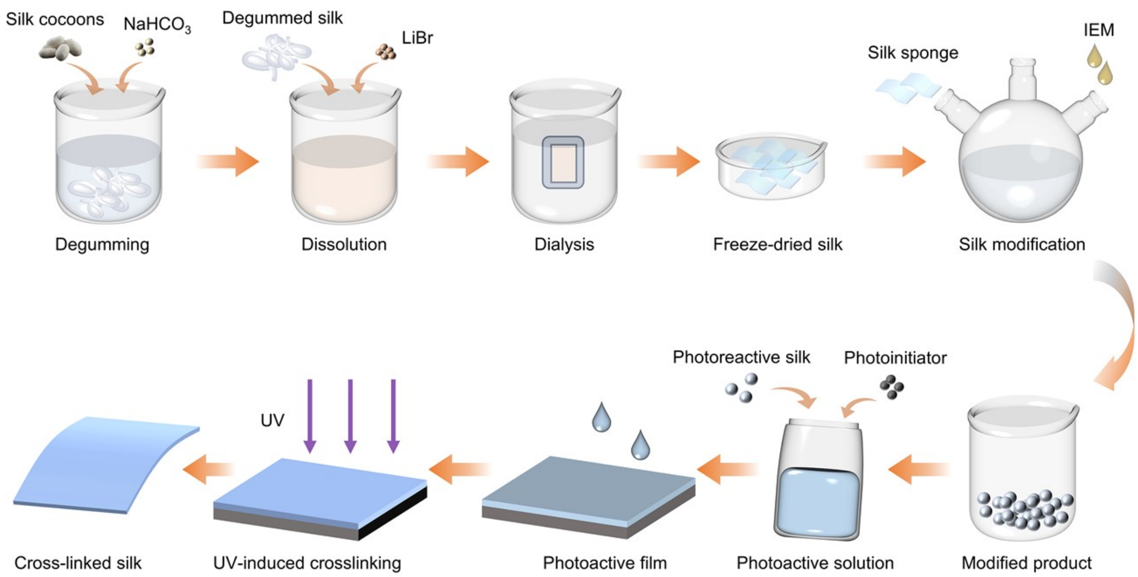

Fig. S1 Fabrication process of the flexible cross-linked silk film.

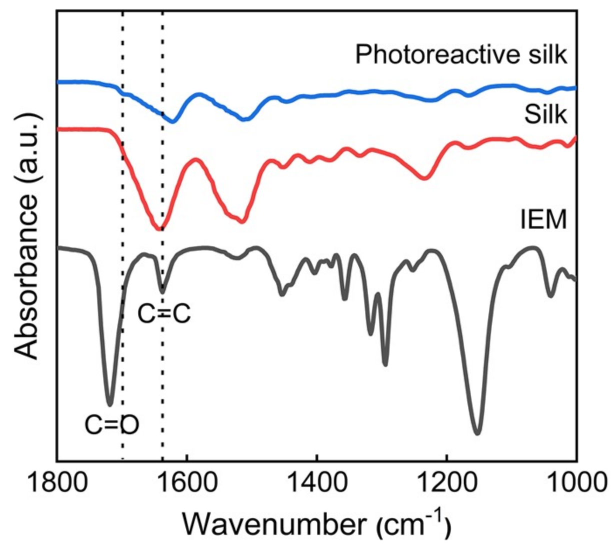

Fig. S2 FTIR spectra of silk, photoreactive silk and the modifying reagent IEM.

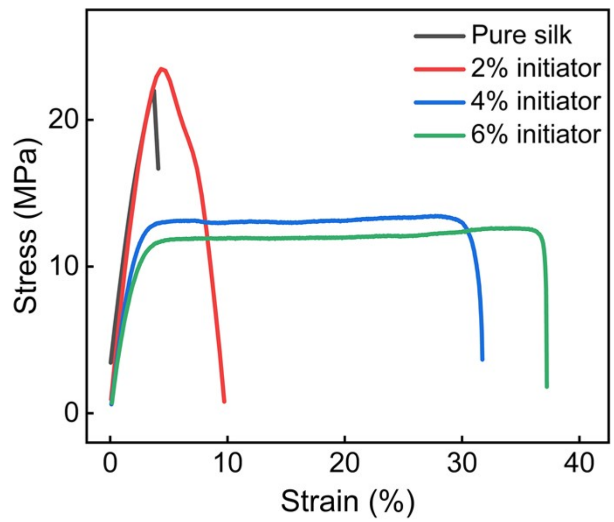

Fig. S3 Stress-strain behavior of pure silk film and cross-linked silk films containing 2 to 6% w/v of photoinitiator.

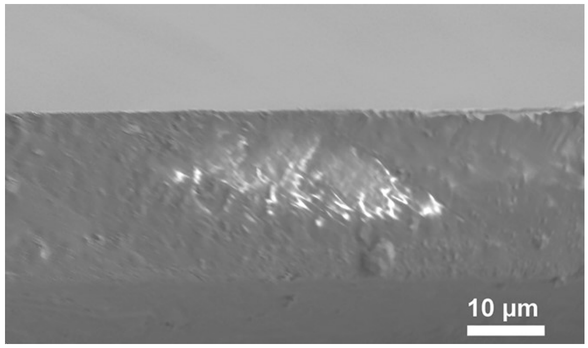

Fig. S4 Cross-sectional image of the cross-linked silk film.

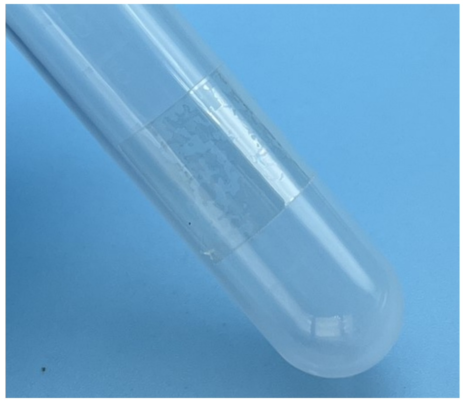

Fig. S5 Photograph of the cross-linked silk film conformably attached to a curved surface.

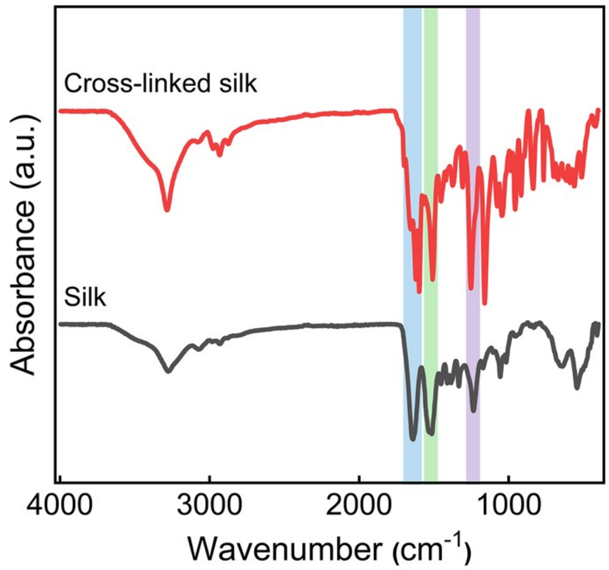

Fig. S6 FTIR spectra of pure silk film and cross-linked silk film.

Table S1. Comparison of properties among PET, PI, PEEK, and this work.

Properties	PET	PI	PEEK	**This work**
Young's modulus (GPa)	2.76–4.14[1]	1.3–4.0[1]	5.2[2]	**0.55**
Elongation at break	20	90	30-40[3]	**31**
Biocompatible	No[4]	No[4]	Yes	**Yes**
Biodegradable	No	No	No	**Yes**

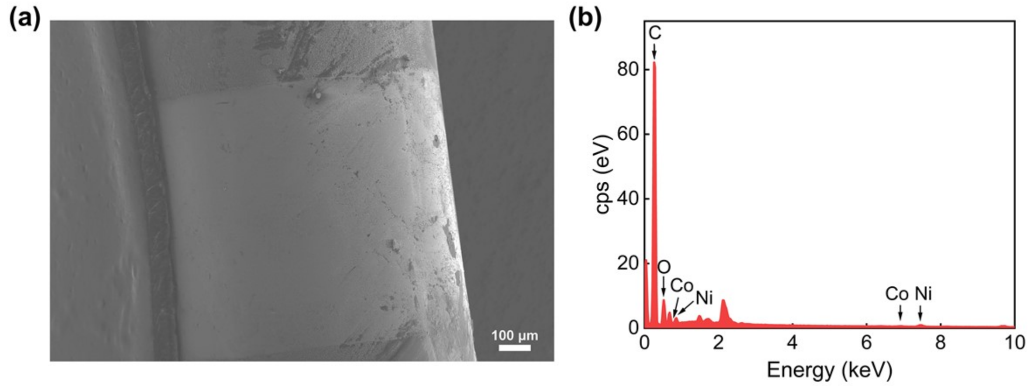

Fig. S7 (a) The surface image of NiCo/cross-linked silk film. (b) EDS analysis of NiCo/cross-linked silk film.

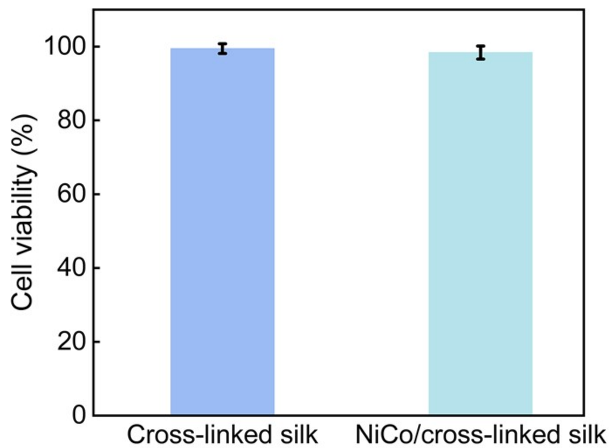

Fig. S8 Cell viability of mouse cardiomyocytes and fibroblasts (1:20) after 48 h cultured on cross-linked silk film and NiCo/cross-linked silk film.

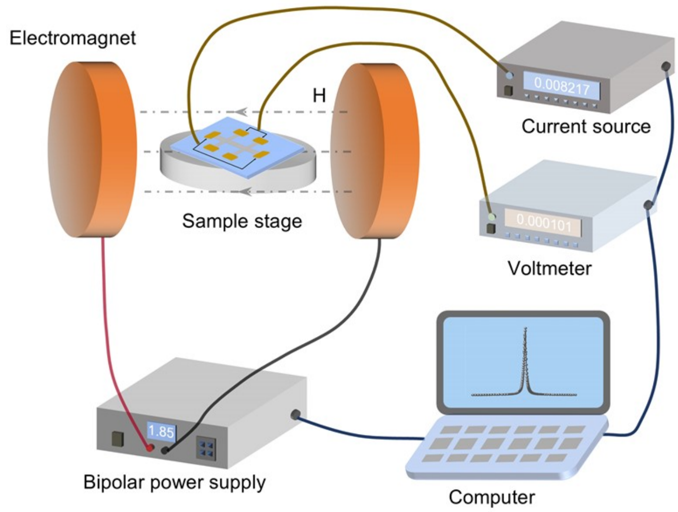

Fig. S9 Schematic illustration of the experimental set-up by using a four-point configuration in the uniform in-plane magnetic field produced by electromagnet.

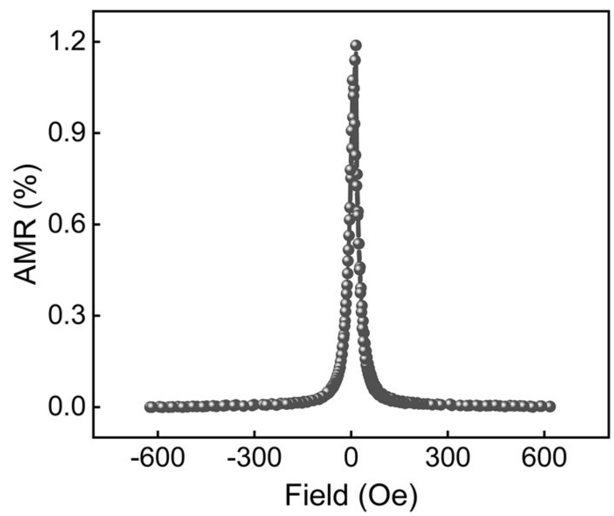

Fig. S10 AMR ratio of NiCo/SiO_2/Si.

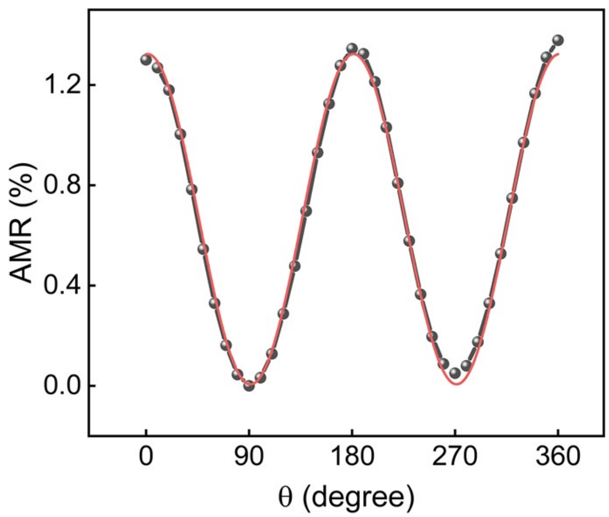

Fig. S11 AMR ratio of the silk-based AMR with various magnetic field angle.

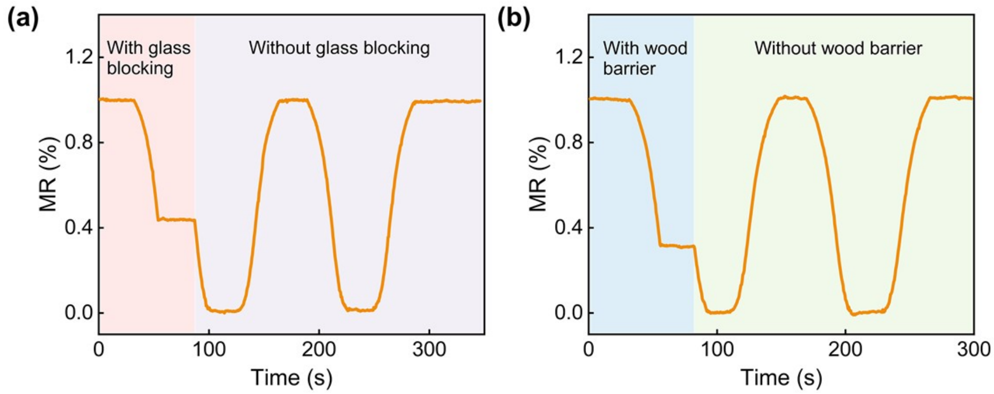

Fig. S12 MR of the silk-based AMR in the case of (a) glass blocking and (b) wood barrier.

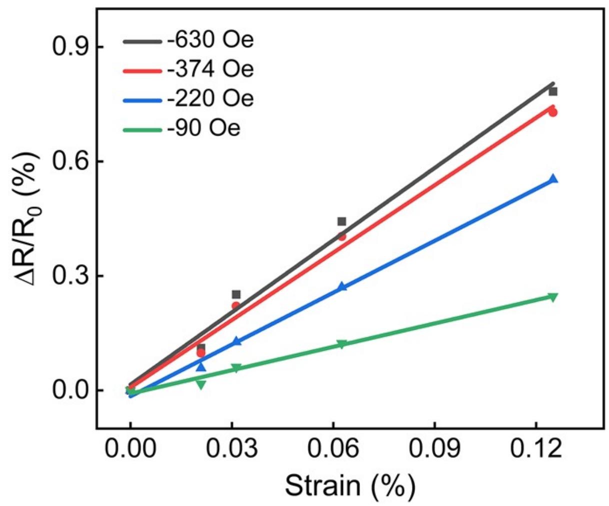

Fig. S13 The change curve of sample resistance with strain of the silk-based AMR at different magnetic fields.

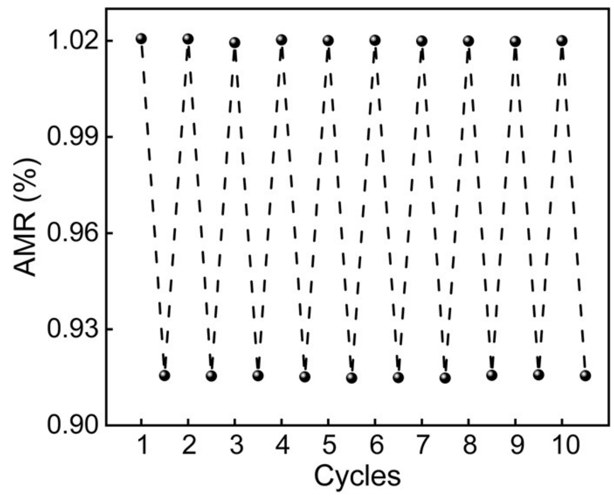

Fig. S14 Reversibility test of the AMR performance of the silk-based AMR with a bending radius of 60 mm.

Reference

1. H. Liu, W. Wei, L. Zhang, J. Xiao, J. Pan, Q. Wu, S. Ma, H. Dong, L. Yu, W. Yang, D. Wei, H. Ouyang and Y. Liu, *Adv. Funct. Mater.*, 2021, **31**, 202104088.
2. S. Singh, C. Prakash and S. Ramakrishna, *Eur. Polym. J.*, 2019, **114**, 234-248.
3. S. M. Kurtz and J. N. Devine, *Biomaterials*, 2007, **28**, 4845-4869.
4. F. Chen, X. Li, G. Liu, J. Zhao, L. Zhao, Y. Shi, Y. Shi, Z. Xu, W. Guo and Y. Liu, *Adv. Mater. Technol.*, 2023, **8**, 202201980.